


 Cite this: *RSC Adv.*, 2024, 14, 7022

# Uric acid quantification *via* colorimetric detection utilizing silver oxide-modified activated carbon nanoparticles functionalized with ionic liquid

 Umar Nishan,<sup>a</sup> Ateeq Ahmed,<sup>a</sup> Nawshad Muhammad,<sup>b</sup> Mohibullah Shah,<sup>c</sup> Muhammad Asad,<sup>a</sup> Naeem Khan,<sup>a</sup> Farman Ullah,<sup>d</sup> Riaz Ullah,<sup>e</sup> Essam A. Ali,<sup>f</sup> Haq Nawaz<sup>g</sup> and Amir Badshah<sup>\*a</sup>

Uric acid (UA) is a significant indicator of human health because it is linked to several diseases, including renal failure, kidney stones, arthritis, and gout. Uric acid buildup in the joints is the source of chronic and painful diseases. When UA is present in large quantities, it causes tissue injury in the joints that are afflicted. In this research, silver oxide-doped activated carbon nanoparticles were synthesized and then functionalized with an ionic liquid. The synthesized nanomaterial assembly was employed as a colorimetric sensing platform for uric acid. Activated carbon offers a large internal surface area that acts as a good carrier for catalytic reactions. A salt-melting approach was used to synthesize the silver oxide-doped activated carbon nanocomposite. The synthesis was confirmed through various techniques, such as UV-vis spectrophotometer, FTIR, XRD, SEM, and EDX. The colorimetric change from blue-green to colorless was observed with the naked eye and confirmed by UV-vis spectroscopy. To obtain the best colorimetric change, several parameters, such as pH, capped NP loading, TMB concentration, hydrogen peroxide concentration, and time, were optimized. The optimized experimental conditions for the proposed sensor were pH 4 with 35  $\mu\text{L}$  of NPs, a 40 mM TMB concentration, and a 4 minutes incubation time. The sensor linear range is 0.001–0.36  $\mu\text{M}$ , with an  $R^2$  value of 0.999. The suggested sensor limits of detection and quantification are 0.207 and 0.69 nM, respectively. Potential interferers, such as ethanol, methanol, urea,  $\text{Ca}^{2+}$ ,  $\text{K}^+$ , and dopamine, did not affect the detection of uric acid.

 Received 25th January 2024  
 Accepted 16th February 2024

DOI: 10.1039/d4ra00659c

[rsc.li/rsc-advances](http://rsc.li/rsc-advances)

## 1 Introduction

The final product of purine derivatives in human metabolism is uric acid (UA). It is eliminated by the intestines and kidneys.<sup>1</sup> Nutrition, age, drug use, and overall health all affect the amount of UA in the human body at varying concentrations. The range of UA in human serum is 120–460  $\mu\text{M}$ .<sup>2</sup> Serious conditions such as Lesch Nyhan syndrome, renal disorders, and gout can be brought on by abnormally high levels of UA.<sup>3</sup> High UA levels, frequently referred to as hyperuricemia, are linked to

hypertension, cardiovascular and cerebrovascular disorders, and metabolic syndrome.<sup>4</sup> Thus, it is very crucial to develop a sensitive, accurate, and rapid platform for the detection of UA.

A number of techniques have been used for the determination of UA, such as enzymatic methods,<sup>5</sup> chemiluminescence,<sup>6</sup> liquid chromatography,<sup>7</sup> and electrochemiluminescence.<sup>8</sup> However, these methods have limited applications because of the high cost and complexity of the procedures, thereby restricting their application in labs with limited resources. In comparison to the previously described methods, the colorimetric biosensor method for UA detection is extremely quick, easy to use, inexpensive, highly selective, and sensitive. Since the discovery of  $\text{Fe}_3\text{O}_4$  nanoparticles as enzyme mimics,<sup>9</sup> an increasing number of scientists have shown that nanozymes possess peroxidase-like activity. They effectively overcome the shortcomings of natural enzymes, such as their high cost, low shelf life, difficult handling, and instability.<sup>10</sup>

Activated carbons (ACs) have recently attracted a lot of attention due to their favorable physico- and electro-chemical characteristics. These include, accessibility, surface functionality, good electrical conductivity, thermal stability, low toxicity, uniform porosity, and high surface area.<sup>11</sup> AC is a material that meets all of the requirements for usage as a catalyst support. In

<sup>a</sup>Department of Chemistry, Kohat University of Science and Technology, Kohat 26000, KP, Pakistan. E-mail: umarnishan85@gmail.com; amirqau@yahoo.com

<sup>b</sup>Department of Dental Materials, Institute of Basic Medical Sciences Khyber Medical University, Peshawar, KPK, Pakistan

<sup>c</sup>Department of Biochemistry, Bahauddin Zakariya University, Multan 66000, Pakistan

<sup>d</sup>Department of Pharmacy, Kohat University of Science and Technology, Kohat 26000, KP, Pakistan

<sup>e</sup>Department of Pharmacognosy, College of Pharmacy, King Saud University, Riyadh, Saudi Arabia

<sup>f</sup>Department of Pharmaceutical Chemistry, College of Pharmacy, King Saud University, Riyadh, Saudi Arabia

<sup>g</sup>School of Chemistry and Chemical Engineering, Huaiyin Normal University, 223300, Huaiyin, Jiangsu, China



comparison to conventional carriers like alumina or silica, ACs offer a larger internal surface area for a higher reaction rate and a lower cost per cubic meter. In the hydrothermal process, the addition of a tiny amount of metal ions to activated carbon led to the creation of carbon nanoparticles and gave them strong peroxidase-like activity and use in various aspects.<sup>12</sup> The ability of iron nanoparticles was increased when they were modified with activated carbon compared to pure activated carbon.<sup>13</sup>

The capability of nanoparticles to facilitate quick electron transport between the electrode and the enzyme's active site is one of its special qualities.<sup>14</sup> Various types of nanoparticles, including gold (AuNPs),<sup>15</sup> zinc-oxide (ZnO-NPs),<sup>16</sup> and iron-oxide (Fe<sub>3</sub>O<sub>4</sub>-NPs),<sup>17</sup> have been used for enzyme immobilization to improve the stability and sensitivity of the activated carbon based biosensors. In addition, modified activated carbons are utilized in a variety of processes, including gas and air purification, water treatment, catalysis, metal extraction, energy storage, and bio and environmental applications. A large variety of chemical substances and bacterial nutrients can be effectively absorbed by AC.<sup>18</sup>

Ionic liquids are of great interest due to their unique properties, including low volatility, relatively strong ionic conductivity, chemical and thermal stability, and the capacity to dissolve a variety of compounds by appropriately altering the anions and cations.<sup>19</sup> They can be used as a capping agent to improve the stability, electrical conductivity and deagglomeration of nanomaterials.<sup>20</sup>

In the current work, we have fabricated silver oxide-doped activated carbon using a salt melting method. The method as opposed to solvent based methods is free from the temperature limitation and can operate on temperatures as high as 1000 °C. Furthermore, the synthesized platform was functionalized with 1-H-3 methyl imidazolium acetate ionic liquid. The novelty of the current work lies in the use of silver oxide-doped activated carbon functionalized with ionic liquid for the colorimetric sensing of uric acid. The reported method is highly sensitive, selective, rapid, and simple. The chromogenic substrate 3,3',5,5'-tetramethylbenzidine (TMB) was used with the support of H<sub>2</sub>O<sub>2</sub>. To obtain the best colorimetric response, various parameters, such as TMB concentration, ionic liquid-coated NPs, incubation time, and pH were optimized. The sensitivity and selectivity of the proposed sensor were also analyzed using the optimum conditions. The optimized platform was used successfully to detect UA in human blood serum samples with excellent sensitivity and selectivity.

## 2 Materials and methods

### 2.1 Chemicals and reagents

Sigma Aldrich provided 3,3',5,5'-tetramethylbenzidine (TMB), sodium hydroxide (NaOH), hydrochloric acid (HCl), silver nitrate (AgNO<sub>3</sub>), and hydrogen peroxide (H<sub>2</sub>O<sub>2</sub>). BioWorld provided PBS in a range of pH levels. All of these compounds were in their pure form and were used without further purification. The solutions were made with deionized water from an Elga Purelab Ultra water deionizer, and the tests were carried out with high-quality glassware. Human serum samples were

collected from a local lab (Al-Habib clinical laboratory) in Kohat and diluted to reduce the serum complexity and also to take advantage of the sensitive nature of the proposed sensor. This work was approved by the ethical committee of the Kohat University of Science and Technology, Kohat KP Pakistan *via* KUST/Ethical Committee/22-12.

### 2.2 Instrumentation

The FTIR spectrometer used was from Agilent Technologies in Danbury, Conn. The FTIR spectra of the materials were obtained using a range of 4000–500 cm<sup>-1</sup>. Scanning electron microscopy (SEM) was used to examine the morphology of silver oxide-doped activated carbon nanoparticles. X-ray powder diffraction (XRD; PAN analytical, X'pert Powder) was used to analyze the size and phase of the synthesized silver oxide-doped activated carbon nanoparticles. On a UV-vis spectrophotometer, the UV-vis spectra of both the silver oxide-doped activated carbon nanoparticles and the experimental materials were recorded (Shimadzu, UV, 1800, Japan).

### 2.3 Synthesis of silver oxide doped activated carbon

An innovative and inexpensive salt melting method was employed to synthesize silver oxide-doped activated carbon nanoparticles by utilizing a modified version of the method described elsewhere.<sup>21,22</sup> Briefly, 5 g of silver nitrate and 10 g of activated carbon were mixed using a mortar and pestle. The combined samples were then placed in a muffle furnace in a crucible with a volume of 30 mL. The mixed sample was stored for four hours after being heated at a rate of 10 °C per minute from room temperature to 800 °C. The muffle furnace's interior was used to cool the activated sample to room temperature. After that, the synthesized NPs were processed for characterization.

### 2.4 Characterization

The prepared nanoparticles were characterized using different techniques. These include Fourier transform infrared spectroscopy (FTIR), scanning electron microscopy (SEM), X-ray diffraction (XRD), thermogravimetric analysis (TGA), EDX, and UV-vis spectroscopy.

### 2.5 Synthesis of ionic liquid

The preparation of 1-H-3 methylimidazolium acetate ionic liquid was done using the modified protocol previously reported by our group.<sup>23,24</sup>

### 2.6 Capping of silver oxide doped activated carbon NPs with ionic liquid

The synthesized platform (silver oxide doped AC) was functionalized by using 1-H-3-methyl imidazolium acetate ionic liquid (IL) as capping and deagglomeration agent. 1 mL of the ionic liquid was mixed with the 6 mg of the synthesized silver-oxide doped activated carbon. Using a pestle and mortar, the mixture was vigorously ground for thirty minutes. The ionic liquid-functionalized Ag<sub>2</sub>O nanoparticles were stored for



further analysis. The functionalization of Ag with ionic liquid was also reported by Asad *et al.*<sup>25</sup>

### 2.7 Colorimetric detection of uric acid

The peroxidase-like activity of silver-doped activated carbon NPs was evaluated through colorimetric detection. In this method, 3,3',5,5'-tetramethylbenzidine (TMB) is expected to be oxidized by H<sub>2</sub>O<sub>2</sub> from a colorless to a blue-green product. The procedure will be carried out as follows: 50  $\mu$ L of stock solution of silver-doped activated carbon NPs and 200  $\mu$ L of TMB (2 mM) and

0.2 mM acetate buffer solution were mixed, followed by the addition of 200  $\mu$ L of hydrogen peroxide. Subsequently, 150  $\mu$ L of UA (0.36  $\mu$ M) was added to the reaction solution and incubated. The expected colorimetric change was observed with the naked eye and confirmed with a UV-vis spectrophotometer.

## 3 Results and discussion

### 3.1 FTIR analysis

Fourier transform infrared spectroscopy was used for the determination of functional groups. Fig. 1(i) demonstrates the FTIR

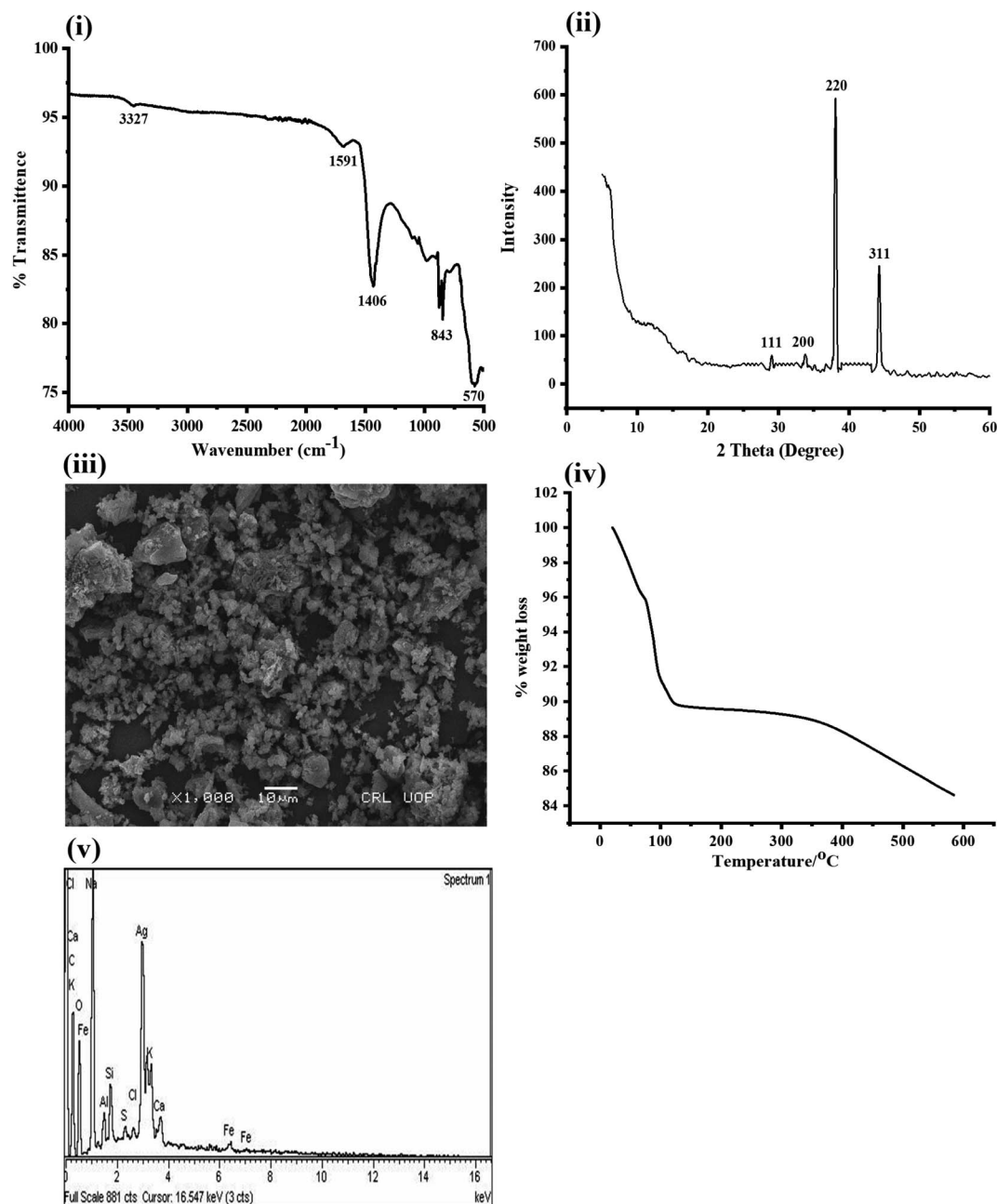


Fig. 1 (i) FTIR spectrum of Ag<sub>2</sub>O-doped activated carbon showing the presence Ag–O bond. (ii) XRD analysis of the synthesized Ag<sub>2</sub>O-doped activated carbon indicating the orthorhombic-phase. (iii) SEM image of the synthesized Ag<sub>2</sub>O-doped activated carbon NPs. (iv) TGA analysis of the prepared Ag<sub>2</sub>O-doped activated carbon NPs. (v) EDX analysis of the prepared Ag<sub>2</sub>O nanoparticles.



spectrum of the prepared silver oxide-doped activated carbon nanoparticles. The peak present at  $3327\text{ cm}^{-1}$  reflect the presence of OH in our synthesized platform. The OH band at  $3327\text{ cm}^{-1}$  usually comes from moisture that is present in the air. The peaks around  $1591\text{ cm}^{-1}$  indicate the presence of C=C in conjugation with other functionalities. The other bands at  $1406\text{ cm}^{-1}$  reflect the presence of alkyl bending functionalities. The band around  $843\text{ cm}^{-1}$  is due to the presence of a C-Cl group present in the activated carbon. The final band at  $570\text{ cm}^{-1}$  can be attributed to the presence of Ag-O in the platform.<sup>26</sup>

**3.1.1 XRD analysis.** Fig. 1(ii) shows the X-ray diffraction pattern of  $\text{Ag}_2\text{O}$ -doped activated carbon NPs. The XRD pattern of the synthesized  $\text{Ag}_2\text{O}$ -doped activated carbon NPs shows two diffraction peaks centered at  $2\theta = 29, 33, 38,$  and  $44$  with miller indices of 111, 200, 220, and 311. The production of  $\text{Ag}_2\text{O}$ -doped activated carbon NPs with an orthorhombic phase is confirmed by the diffraction peaks in the XRD pattern of synthesized  $\text{Ag}_2\text{O}$ -doped activated carbon NPs (JCPDS No. 047-0561).<sup>27</sup> The average crystal sizes of orthorhombic-phase  $\text{Ag}_2\text{O}$ -doped activated carbon NPs were estimated to be about 17 nm.

**3.1.2 SEM analysis.** Fig. 1(iii) shows the SEM image of the synthesized  $\text{Ag}_2\text{O}$ -doped activated carbon NPs. The image shows that the  $\text{Ag}_2\text{O}$  nanoparticles distributed homogeneously on the surface of the activated carbon. Here the activated carbon plays important role in keeping the  $\text{Ag}_2\text{O}$  nanoparticles in non-agglomerated form, As a result the activity of our synthesized platform is very high, which act as nanoenzyme.<sup>28</sup>

**3.1.3 TGA analysis.** The thermal degradation behavior (TGA curve) of the silver oxide-doped activated carbon NPs is shown in Fig. 1(iv). It is observed from the TGA curve that weight loss of the NPs occurred throughout the temperature range of 30 to 600 °C. The first weight loss can be attributed to the loss of moisture. The second weight loss can attributed to the organic moieties present in the activated carbon.<sup>29</sup>

**3.1.4 EDX spectrum.** The prepared silver oxide-doped activated carbon nanoparticles were utilized for the study of the energy-dispersive X-ray spectrum. Ag peaks can be clearly seen in Fig. 1(v). In the EDX spectrum of silver oxide-doped activated carbon nanoparticles, the peaks for the elements O and C could be seen. Using an EDX spectrum, the chemical

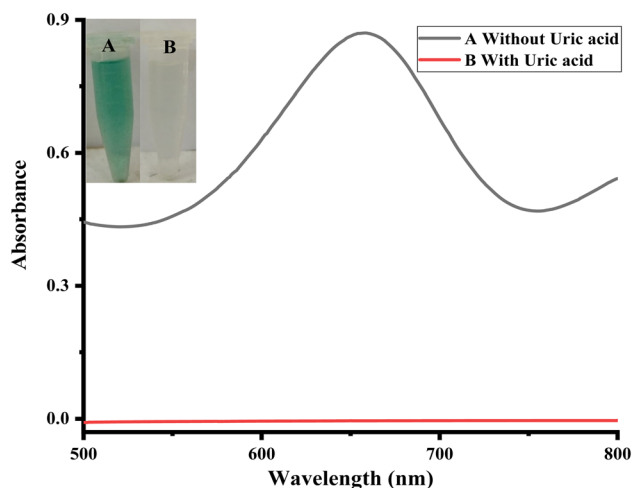


Fig. 2 Colorimetric detection of uric acid [conditions: capping 35  $\mu\text{L}$ , PBS 550  $\mu\text{L}$ , TMB 200  $\mu\text{L}$  (40 mM),  $\text{H}_2\text{O}_2$  90  $\mu\text{L}$  (25 mM), uric acid 150  $\mu\text{L}$  (0.36  $\mu\text{M}$ )].

compositions of the  $\text{Ag}_2\text{O}/\text{AC}$  NPs were examined. The composites contained Ag 3.79% in atomic percentage, 32.66% oxygen, and 51.64% carbon.<sup>3</sup> Various other elements, such as Na, Al, Si, etc., were also detected in minor quantities (Table 1), which are typically observed in activated carbon depending on the source of its origin and the reagents used for its preparation.

### 3.2 Colorimetric detection of uric acid

For the detection of uric acid, a simple and selective colorimetric technique based on  $\text{Ag}_2\text{O}$ -doped activated carbon NPs was used. Fig. 2 depicts the optical sensing and UV-vis absorption spectra for the reaction mixture. The mimic enzyme with the assistance of hydrogen peroxide converts the colorless TMB solution to blue-green color ( $\text{TMB}_{\text{oxi}}$ ). The addition of uric acid to the reaction mixture resulted in the reduction of oxidized TMB to reduced form. This transformation was observed with the naked eye and the color of TMB solution diminished. The colorimetric change was confirmed through a UV-vis spectrophotometer as shown in the Figure.

### 3.3 Ionic liquid-capped $\text{Ag}_2\text{O}/\text{activated carbon NPs}$ based sensing of UA

In this work, we propose a simple, sensitive, and selective colorimetric approach for uric acid detection based on  $\text{Ag}_2\text{O}$ -doped activated carbon NPs.  $\text{Ag}_2\text{O}/\text{AC}$  NPs have intrinsic oxidase-like activity, and in the presence of hydrogen peroxide, TMB can be oxidized from colorless to blue-green oxidized TMB, generating an absorption peak at 652 nm as shown in Scheme 1. During the course of the reaction, the mimic enzyme catalyzes the production of OH free radicals from  $\text{H}_2\text{O}_2$ . The generated free radicals oxidize the TMB, and hence a blue-green color is produced, indicating the presence of an oxidized form of TMB. The reduction of oxidized TMB after the addition of uric acid in the presence of  $\text{Ag}_2\text{O}/\text{AC}$  NPs decreased proportionally until it became completely transparent. During the

Table 1 EDX analysis showing the elemental composition of the synthesized  $\text{Ag}_2\text{O}$ -doped AC NPs

Element	Weight%	Atomic%
C	33.56	51.64
O	28.42	32.66
Na	8.01	6.80
Al	1.24	0.90
Si	1.96	1.36
S	0.44	0.27
Cl	0.24	0.13
K	2.68	1.34
Ca	1.47	0.72
Fe	1.11	0.39
Ag	20.87	3.79
Totals	100.0	100.0



reduction of TMB to its colorless form, the uric acid acts as a reducing agent. It reduces the oxidized TMB to its original, colorless form and itself oxidizes to allantoin along with the production of  $\text{CO}_2$ , as shown in Scheme 1.

### 3.4 Optimization of parameters

**3.4.1 Capped NPs amount optimization.** The amount of capped nanoparticles was optimized, as shown in Fig. 3(i). Different amounts of NPs were taken in an Eppendorf tube, and the best colorimetric response was obtained at 35  $\mu\text{L}$  of NPs, as shown in Fig. 3(i). When the amount of NPs was either increased or decreased from 35 mg, the colorimetric response was not as good as in the case of 35 mg. So a 35  $\mu\text{L}$  amount was considered the optimum amount and was used in further experiments. Previously, Nishan *et al.* reported that 40  $\mu\text{L}$  of IL-capped NiNPs was optimal for the detection of uric acid.<sup>30</sup>

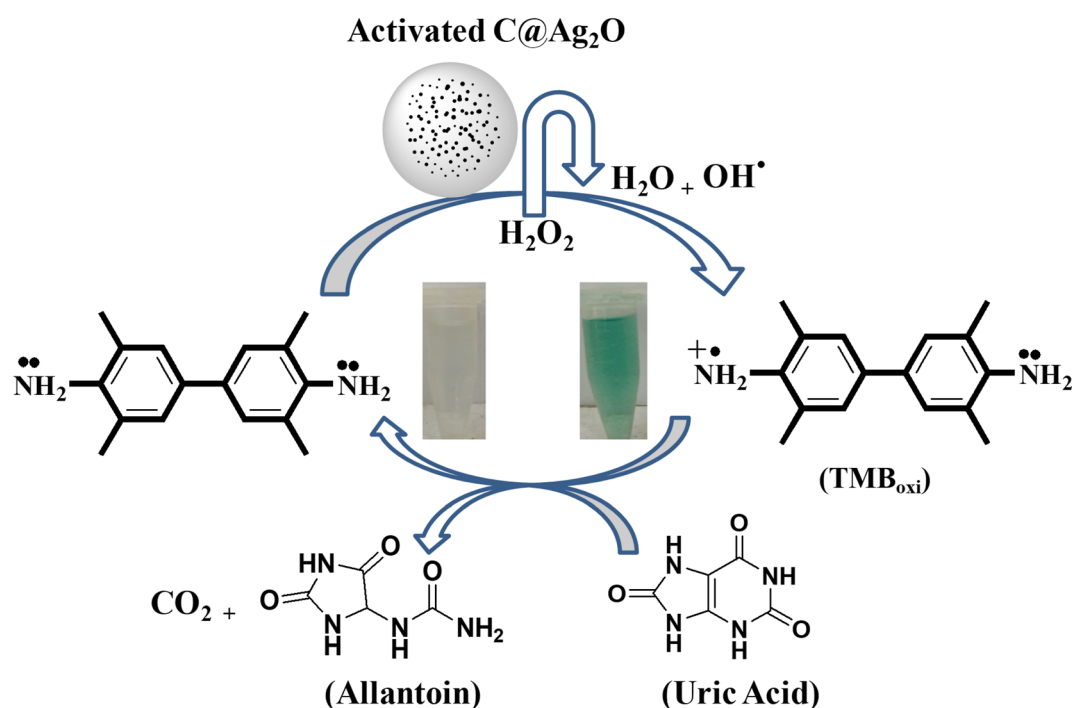
**3.4.2 pH optimization.** The pH of the solution is critical in the biosensor system. It changes the biosensor's efficiency by either increasing or decreasing it. As shown in Fig. 3(ii), the influence of pH on the sensor was investigated using PBS buffer solution at various pH levels ranging from 3 to 11. PBS buffer solution was used to optimize the pH, while hydrochloric acid and sodium hydroxide solutions were used to change the pH. At pH 4, there was a good response. A modest colorimetric change was found at pH 3 and pH 5. There was no colorimetric change at higher pH, ranging from 6 to 11, and at lower pH 3, implying that pH 4 provided the optimum colorimetric response. As a result, pH 4 was chosen as the best pH for further experiments. pH less than 4 was used in the literature because catalytic activity in acidic solutions was substantially higher than in neutral and basic solutions.

**3.4.3 TMB optimization.** The TMB concentration was also optimized to achieve the best colorimetric change. TMB solutions of various concentrations were prepared, ranging from 10 mM to 70 mM. The sensor responded best at a 40 mM TMB concentration, and when uric acid was added, the color became light and transparent. The colorimetric reaction was not as good at lower concentrations or higher concentrations as 40 mM. For the rest of the experiments, a concentration of 40 mM TMB was chosen as the optimal concentration, as shown in Fig. 3(iii).

**3.4.4 Hydrogen peroxide optimization.** The hydrogen peroxide concentration was also optimized to obtain the best colorimetric response, as shown in the figure. Different concentrations of hydrogen peroxide were formed, ranging from 10 mM to 40 mM, and the best colorimetric response was obtained at a 25 mM concentration. At concentrations higher or lower than 25 mM, no significant colorimetric change was observed, so the 25 mM concentration was chosen as the optimum concentration, and further experiments were performed using this optimum concentration, as shown in Fig. 3(iv).

**3.4.5 Time optimization.** The impact of time on the sensor was also investigated at intervals ranging from 1 to 6 minutes. The best response was obtained after 4 minutes of incubation because all of the capped NPs were consumed in the reaction, no additional changes were detected after 4 minutes, and the color became fully transparent. As a result, for the remaining experiments, 4 minutes was chosen as the optimal time, as shown in Fig. 3(v).

**3.4.6 Colorimetric and spectrophotometric detection of uric acid.** To detect different concentrations of uric acid, a simple colorimetric test was used directly using the  $\text{Ag}_2\text{O}$ -



Scheme 1 Ionic liquid capped  $\text{Ag}_2\text{O}$ /activated carbon NPs as a sensing platform for uric acid.



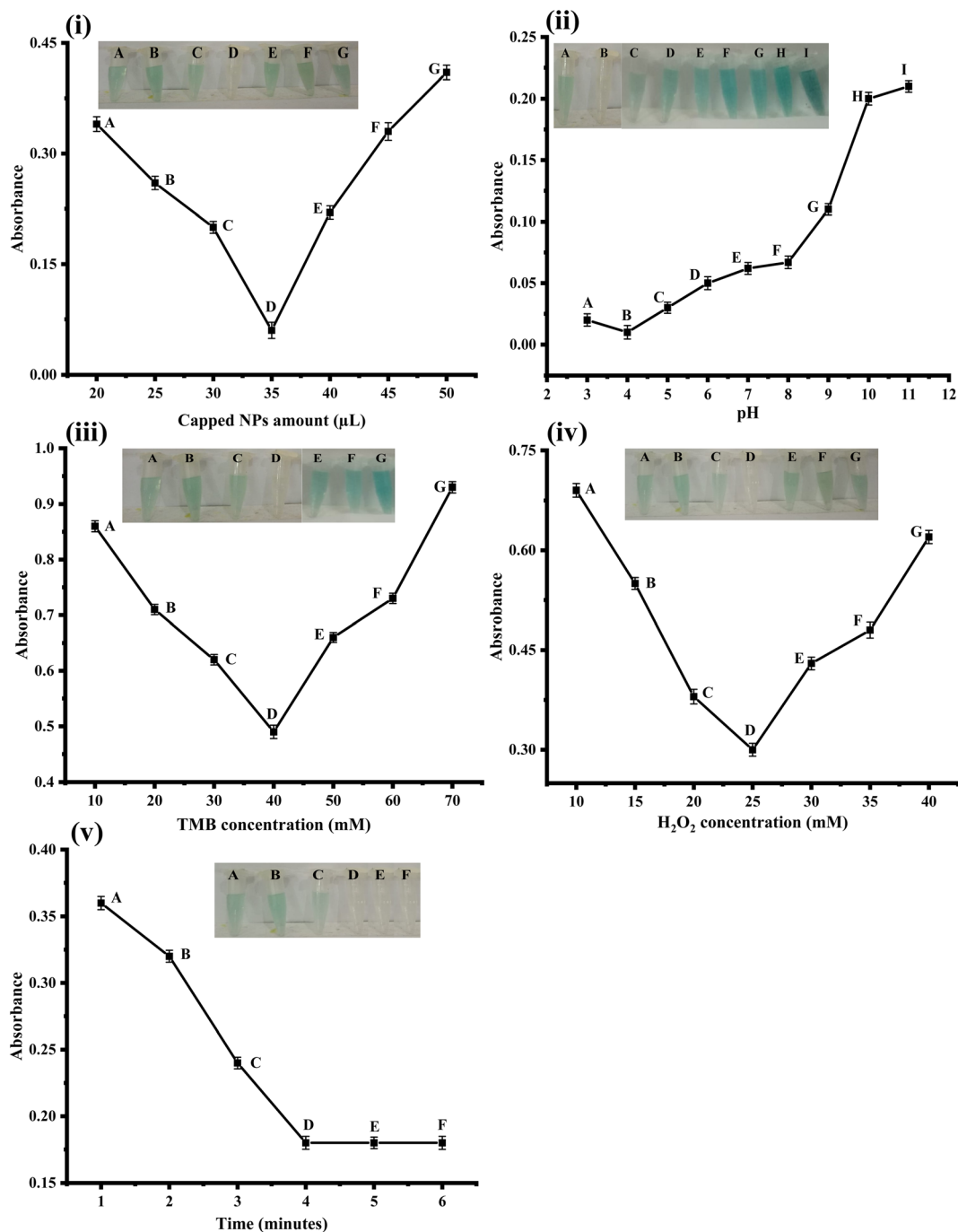


**Fig. 3** (i) Optimization of capped amount [conditions: capping 35  $\mu\text{L}$ , PBS 550  $\mu\text{L}$ , TMB 200  $\mu\text{L}$  (40 mM), H<sub>2</sub>O<sub>2</sub> 90  $\mu\text{L}$  (25 mM), uric acid 150  $\mu\text{L}$  (0.36  $\mu\text{M}$ )]. (ii) pH optimization of the proposed sensor [conditions: capping 35  $\mu\text{L}$ , PBS 550  $\mu\text{L}$ , TMB 200  $\mu\text{L}$  (40 mM), H<sub>2</sub>O<sub>2</sub> 90  $\mu\text{L}$  (25 mM), Uric acid 150  $\mu\text{L}$  (0.36  $\mu\text{M}$ )]. (iii) TMB optimization of the proposed sensor [conditions: capping 35  $\mu\text{L}$ , PBS 550  $\mu\text{L}$ , TMB 200  $\mu\text{L}$  (40 mM), H<sub>2</sub>O<sub>2</sub> 90  $\mu\text{L}$  (25 mM), uric acid 150  $\mu\text{L}$  (0.36  $\mu\text{M}$ )]. (iv) Hydrogen peroxide optimization of the proposed sensor [conditions: capping 35  $\mu\text{L}$ , PBS 550  $\mu\text{L}$ , TMB 200  $\mu\text{L}$  (40 mM), H<sub>2</sub>O<sub>2</sub> 90  $\mu\text{L}$  (25 mM), uric acid 150  $\mu\text{L}$  (0.36  $\mu\text{M}$ )]. (v) Time optimization of the proposed sensor [conditions: capping 35  $\mu\text{L}$ , PBS 550  $\mu\text{L}$ , TMB 200  $\mu\text{L}$  (40 mM), H<sub>2</sub>O<sub>2</sub> 90  $\mu\text{L}$  (25 mM), uric acid 150  $\mu\text{L}$  (0.36  $\mu\text{M}$ )].

doped activated carbon NPs under optimum experimental conditions. For the quantitative assessment of uric acid, a sensitive and selective colorimetric technique based on the relationship between uric acid concentration and absorbance intensity at 652 nm was used. Various uric acid concentrations were used to test the sensitivity of the sensor designed for uric

acid detection. Fig. 4(i) and (ii) show the response of colorimetric biosensors to various uric acid concentrations. The sensor response and peak intensity were high at lower uric acid concentrations, but they dropped linearly as the uric acid concentration increased. With an  $R^2$  value of 0.999, this method was able to detect uric acid with a linear range of 0.001–0.36  $\mu\text{M}$ .

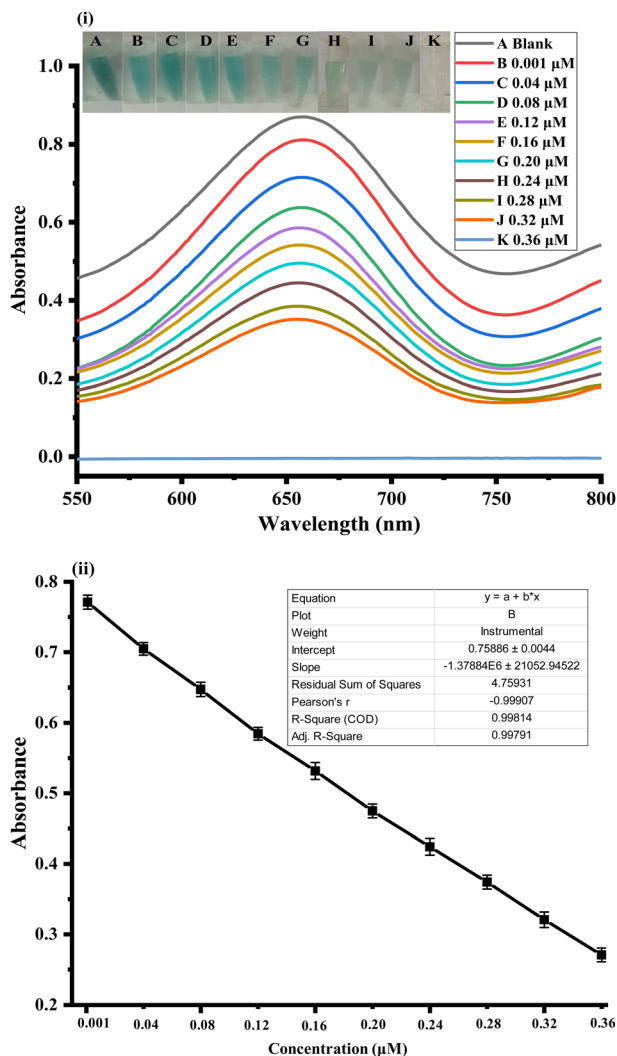


Fig. 4 (i) Typical UV-vis spectra of the proposed assay at various UA concentrations (0.001–0.36  $\mu\text{M}$ ),  $\text{Ag}_2\text{O}/\text{AC}$ ,  $\text{H}_2\text{O}_2$ , and TMB. (ii) Relationship between the UA concentration and the absorption spectra peak at 652 nm. The error bars show the standard deviations of three different measurements.

The limits of quantification (LOQ) and detection (LOD) were determined to be 0.69 and 0.207 nM, respectively. In comparison to other previously reported detection methods, the

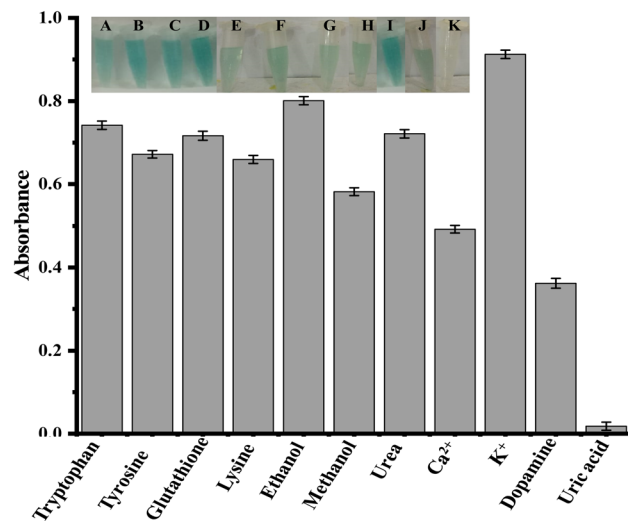


Fig. 5 Selectivity study of the proposed sensor at optimized conditions [conditions: capping 35  $\mu\text{L}$ , PBS 550  $\mu\text{L}$ , TMB 200  $\mu\text{L}$  (40 mM),  $\text{H}_2\text{O}_2$  90  $\mu\text{L}$  (25 mM), tryptophan, tyrosine, glutathione, lysine, ethanol, methanol, urea,  $\text{Ca}^{2+}$ ,  $\text{K}^+$ , and dopamine 150  $\mu\text{L}$  (0.36  $\mu\text{M}$ )].

proposed colorimetric method had the advantages of a low detection limit, low cost, and direct eye observation. This shows that our sensor can work at both high and low concentrations. Based on the linear range and limit of detection, the following Table 2 compares previously reported colorimetric methods with the present study for uric acid detection.

### 3.5 Selectivity study of the proposed sensor

Fig. 5 shows that the selectivity of the proposed sensor was tested with potential interfering species such as tryptophan, tyrosine, glutathione, lysine, ethanol, methanol, urea,  $\text{Ca}^{2+}$ ,  $\text{K}^+$ , and dopamine. Tryptophan, tyrosine, glutathione, lysine, ethanol, methanol, urea,  $\text{Ca}^{2+}$ ,  $\text{K}^+$ , and dopamine have relatively high absorption values when compared to uric acid. The absorption value at 652 nm decreases when uric acid is added, as indicated in Fig. 5. As shown in Fig. 5, there was no significant decrease in absorbance when other interfering species were added. So it is concluded that, in the presence of other

Table 2 Comparison of some of the colorimetric biosensors for uric acid with recently reported studies

S. No	Materials used	Method	Limit of detection ( $\mu\text{M}$ )	Linear range ( $\mu\text{M}$ )	References
1	Ag nanoprisms	Colorimetric	0.7	1 to 40	31
2	MIL-53(Fe)	Colorimetric	1.3	4.5 to 60	32
3	$\text{MoS}_2$ nanoflakes	Colorimetric	0.3	0.5–100	33
4	Chitosan stabilized Au NPs	Colorimetric	0.04	0.1 to 30	34
5	AuNPs-GO	Colorimetric	0.06	1 to 40	35
6	CuS NPs	Colorimetric	1	1–100	36
7	PtNPs	Colorimetric	4.2	1–8000	37
8	$\mu\text{PADs}$ modified with chitosan	Colorimetric	37	130–380	38
9	$\text{Fe}_3\text{O}_4@/\text{MnO}_2$	Colorimetric	0.27	1–70	39
10	IL- $\text{Ag}_2\text{O}$ /activated carbon NPs	Colorimetric	0.00021	0.001–0.36	This work



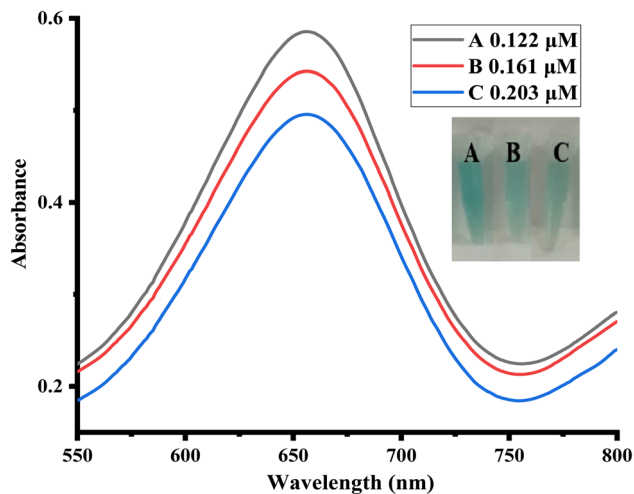


Fig. 6 UV-vis spectra of uric acid detection in human blood serum samples ( $n = 3$ ) by the dilution of the samples in line with the linear range of the fabricated sensor.

interfering substances, our proposed sensor can detect uric acid in the presence of other potential interfering substances.

### 3.6 Applications of the proposed sensor

The human serum samples that were collected from the local lab were strategically diluted to bring their uric acid concentration within the linear range of the fabricated sensor. Briefly, using the previously drawn calibration plots and varying uric acid concentrations under the same experimental conditions. The concentration of uric acid in human blood serum samples was determined as shown in Fig. 6. Through this procedure, the values of uric acid in diluted serum samples were calculated to be 0.122, 0.161, and 0.203  $\mu\text{M}$ .

## 4 Conclusion

In the present work, silver oxide-doped activated carbon nanoparticles were synthesized successfully by simple salt-melting. The functionalization of the synthesized material was done with an ionic liquid to achieve deagglomeration and better conductivity. The platform was successfully employed for the colorimetric detection of uric acid with exceptional sensitivity and selectivity. Comprehensive optimization experiments were performed to get the optimized conditions for the proposed sensor. The proposed sensor was applied to human serum samples for the successful detection of uric acid. The synthesized platform demonstrated intrinsic peroxidase-like activity. The utilization of silver oxide-doped activated carbon nanoparticles as peroxidase mimics for UA determination is thus considered a potential technique for bioassays and medical diagnostics.

## Conflicts of interest

The authors declare that there is no conflict of interests.

## Acknowledgements

Authors wish to thanks Researchers Supporting Project Number (RSP2024R45) at King Saud University Riyadh Saudi Arabia for financial support.

## References

- 1 S.-H. Huang, Y.-C. Shih, C.-Y. Wu, C.-J. Yuan, Y.-S. Yang, Y.-K. Li and T.-K. Wu, Detection of serum uric acid using the optical polymeric enzyme biochip system, *Biosens. Bioelectron.*, 2004, **19**(12), 1627–1633.
- 2 X. Wang, Z. Li, J. Lai, X. Tang and P. Qiu, Sensitive and highly selective biosensor based on triangular Au nanoplates for detection of uric acid in human serum, *Chem. Afr.*, 2018, **1**(1), 29–35.
- 3 J. Choi, H. Lee, Y. Park, S. Kim, B. Kim, K. An, B. Kim and S. Jung, Application of silver and silver oxide nanoparticles impregnated on activated carbon to the degradation of bromate, *J. Nanosci. Nanotechnol.*, 2016, **16**(5), 4493–4497.
- 4 N. Dhaun, J.-L. Vachier, R. L. Benza, R. Naeije, L.-J. Hwang, X. Liu, S. Teal and D. J. Webb, Endothelin antagonism and uric acid levels in pulmonary arterial hypertension: clinical associations, *J. Heart Lung Transplant.*, 2014, **33**(5), 521–527.
- 5 Y. Jiang, A. Wang and J. Kan, Selective uricase biosensor based on polyaniline synthesized in ionic liquid, *Sens. Actuators, B*, 2007, **124**(2), 529–534.
- 6 T. Zhang, X. Sun and B. Liu, Synthesis of positively charged CdTe quantum dots and detection for uric acid, *Spectrochim. Acta, Part A*, 2011, **79**(5), 1566–1572.
- 7 Y. Zuo, Y. Yang, Z. Zhu, W. He and Z. Aydin, Determination of uric acid and creatinine in human urine using hydrophilic interaction chromatography, *Talanta*, 2011, **83**(5), 1707–1710.
- 8 Y. Tao, X. Zhang, J. Wang, X. Wang and N. Yang, Simultaneous determination of cysteine, ascorbic acid and uric acid by capillary electrophoresis with electrochemiluminescence, *J. Electroanal. Chem.*, 2012, **674**, 65–70.
- 9 L. Gao, J. Zhuang, L. Nie, J. Zhang, Y. Zhang, N. Gu, T. Wang, J. Feng, D. Yang and S. Perrett, Intrinsic peroxidase-like activity of ferromagnetic nanoparticles, *Nat. Nanotechnol.*, 2007, **2**(9), 577–583.
- 10 Q. Wang, H. Wei, Z. Zhang, E. Wang and S. Dong, Nanozyme: An emerging alternative to natural enzyme for biosensing and immunoassay, *TrAC, Trends Anal. Chem.*, 2018, **105**, 218–224.
- 11 M. Sevilla and A. B. Fuertes, Direct synthesis of highly porous interconnected carbon nanosheets and their application as high-performance supercapacitors, *ACS Nano*, 2014, **8**(5), 5069–5078.
- 12 Y.-W. Bao, X.-W. Hua, H.-H. Ran, J. Zeng and F.-G. Wu, Metal-doped carbon nanoparticles with intrinsic peroxidase-like activity for colorimetric detection of  $\text{H}_2\text{O}_2$  and glucose, *J. Mater. Chem. B*, 2019, **7**(2), 296–304.
- 13 B. Deng, M. Caviness and Z. Gu, *Arsenic Removal by Activated Carbon-Based Materials*, ACS Publications, 2005.



- 14 P. Pandey, M. Datta and B. Malhotra, Prospects of nanomaterials in biosensors, *Anal. Lett.*, 2008, **41**(2), 159–209.
- 15 P. Pandey, S. P. Singh, S. K. Arya, V. Gupta, M. Datta, S. Singh and B. D. Malhotra, Application of thiolated gold nanoparticles for the enhancement of glucose oxidase activity, *Langmuir*, 2007, **23**(6), 3333–3337.
- 16 A. Wei, X. W. Sun, J. Wang, Y. Lei, X. Cai, C. M. Li, Z. Dong and W. Huang, Enzymatic glucose biosensor based on ZnO nanorod array grown by hydrothermal decomposition, *Appl. Phys. Lett.*, 2006, **89**(12), 123902.
- 17 J. Wang, X. W. Sun, A. Wei, Y. Lei, X. Cai, C. M. Li and Z. L. Dong, Zinc oxide nanocomb biosensor for glucose detection, *Appl. Phys. Lett.*, 2006, **88**(23), 233106.
- 18 R. Al-Gaashani, D. Almasri, B. Shomar and V. Kochkodan, Preparation and properties of novel activated carbon doped with aluminum oxide and silver for water treatment, *J. Alloys Compd.*, 2021, **858**, 158372.
- 19 J. P. Hallett and T. Welton, Room-temperature ionic liquids: solvents for synthesis and catalysis. 2, *Chem. Rev.*, 2011, **111**(5), 3508–3576.
- 20 T. Li, Y. Li, Y. Zhang, C. Dong, Z. Shen and A. Wu, A colorimetric nitrite detection system with excellent selectivity and high sensitivity based on Ag@Au nanoparticles, *Analyst*, 2015, **140**(4), 1076–1081.
- 21 X. Liu, N. Fechner and M. Antonietti, Salt melt synthesis of ceramics, semiconductors and carbon nanostructures, *Chem. Soc. Rev.*, 2013, **42**(21), 8237–8265.
- 22 J.-F. Ni, H.-H. Zhou, J.-T. Chen and X.-X. Zhang, Molten salt synthesis and electrochemical properties of spherical LiFePO<sub>4</sub> particles, *Mater. Lett.*, 2007, **61**(4–5), 1260–1264.
- 23 U. Nishan, F. Bashir, N. Muhammad, N. Khan, A. Rahim, M. Shah, R. Nazir and M. Sayed, Ionic liquid as a moderator for improved sensing properties of TiO<sub>2</sub> nanostructures for the detection of acetone biomarker in diabetes mellitus, *J. Mol. Liq.*, 2019, **294**, 111681.
- 24 U. Nishan, U. Sabba, A. Rahim, M. Asad, M. Shah, A. Iqbal, J. Iqbal and N. Muhammad, Ionic liquid tuned titanium dioxide nanostructures as an efficient colorimetric sensing platform for dopamine detection, *Mater. Chem. Phys.*, 2021, **262**, 124289.
- 25 M. Asad, N. Muhammad, N. Khan, M. Shah, M. Khan, M. Khan, A. Badshah, Z. Latif and U. Nishan, Colorimetric acetone sensor based on ionic liquid functionalized drug-mediated silver nanostructures, *J. Pharm. Biomed. Anal.*, 2022, **221**, 115043.
- 26 S. N. Islam, S. M. A. Naqvi, S. Parveen and A. Ahmad, Application of mycogenic silver/silver oxide nanoparticles in electrochemical glucose sensing; alongside their catalytic and antimicrobial activity, *3 Biotech*, 2021, **11**(7), 1–11.
- 27 M. Alam, A. M. Asiri, M. Uddin, M. Islam, M. R. Awual and M. M. Rahman, Detection of uric acid based on doped ZnO/Ag<sub>2</sub>O/Co<sub>3</sub>O<sub>4</sub> nanoparticle loaded glassy carbon electrode, *New J. Chem.*, 2019, **43**(22), 8651–8659.
- 28 M. M. Rahman, S. B. Khan, A. Jamal, M. Faisal and A. M. Asiri, Highly sensitive methanol chemical sensor based on undoped silver oxide nanoparticles prepared by a solution method, *Microchim. Acta*, 2012, **178**(1), 99–106.
- 29 U. Nishan, R. Gul, N. Muhammad, M. Asad, A. Rahim, M. Shah, J. Iqbal, J. Uddin and S. Shujah, Colorimetric based sensing of dopamine using ionic liquid functionalized drug mediated silver nanostructures, *Microchem. J.*, 2020, **159**, 105382.
- 30 U. Nishan, W. Ullah, N. Muhammad, M. Asad, S. Afridi, M. Khan, M. Shah, N. Khan and A. Rahim, Development of a nonenzymatic colorimetric sensor for the detection of uric acid based on ionic liquid-mediated nickel nanostructures, *ACS omega*, 2022, **7**(30), 26983–26991.
- 31 D. Wu, H.-F. Lu, H. Xie, J. Wu, C.-M. Wang and Q.-L. Zhang, Uricase-stimulated etching of silver nanoprisms for highly selective and sensitive colorimetric detection of uric acid in human serum, *Sens. Actuators, B*, 2015, **221**, 1433–1440.
- 32 J. Lu, Y. Xiong, C. Liao and F. Ye, Colorimetric detection of uric acid in human urine and serum based on peroxidase mimetic activity of MIL-53 (Fe), *Anal. Methods*, 2015, **7**(23), 9894–9899.
- 33 X. Wang, Q. Yao, X. Tang, H. Zhong, P. Qiu and X. Wang, A highly selective and sensitive colorimetric detection of uric acid in human serum based on MoS<sub>2</sub>-catalyzed oxidation TMB, *Anal. Bioanal. Chem.*, 2019, **411**(4), 943–952.
- 34 F. Li, T. He, S. Wu, Z. Peng, P. Qiu and X. Tang, Visual and colorimetric detection of uric acid in human serum and urine using chitosan stabilized gold nanoparticles, *Microchem. J.*, 2021, **164**, 105987.
- 35 S. Kumar, P. Bhushan and S. Bhattacharya, Development of a paper-based analytical device for colorimetric detection of uric acid using gold nanoparticles–graphene oxide (AuNPs–GO) conjugates, *Anal. Methods*, 2016, **8**(38), 6965–6973.
- 36 W. Xue, T. Cheng-Ling, L. Jia-Jun, H.-Z. ZHANG and W. Jian, Ultra-small CuS nanoparticles as peroxidase mimetics for sensitive and colorimetric detection of uric acid in human serum, *Chin. J. Anal. Chem.*, 2018, **46**(5), e1825–e1831.
- 37 M. Ali, M. A. U. Khalid, I. Shah, S. W. Kim, Y. S. Kim, J. H. Lim and K. H. Choi, based selective and quantitative detection of uric acid using citrate-capped Pt nanoparticles (PtNPs) as a colorimetric sensing probe through a simple and remote-based device, *New J. Chem.*, 2019, **43**(20), 7636–7645.
- 38 E. F. Gabriel, P. T. Garcia, T. M. Cardoso, F. M. Lopes, F. T. Martins and W. K. Coltro, Highly sensitive colorimetric detection of glucose and uric acid in biological fluids using chitosan-modified paper microfluidic devices, *Analyst*, 2016, **141**(15), 4749–4756.
- 39 W. Yang, J. Fei, W. Xu, H. Jiang, M. Sakran, J. Hong, W. Zhu and X. Zhou, A biosensor based on the biomimetic oxidase Fe<sub>3</sub>O<sub>4</sub>@ MnO<sub>2</sub> for colorimetric determination of uric acid, *Colloids Surf., B*, 2022, **212**, 112347.

